Bioinspiration & Biomimetics

PAPER

Reversible adhesion to rough surfaces both in and out of water, inspired by the clingfish suction disc

RECEIVED
4 May 2019

REVISED
23 September 2019

ACCEPTED FOR PUBLICATION
25 September 2019

PUBLISHED
25 October 2019

Jessica A Sandoval[1], Saurabh Jadhav[1], Haocheng Quan[1], Dimitri D Deheyn[2] and Michael T Tolley[1,3]

[1] Department of Mechanical and Aerospace Engineering, University of California San Diego, 9500 Gilman Dr., La Jolla, CA 92093, United States of America
[2] Marine Biology Research Division, Scripps Institution of Oceanography, 9500 Gilman Dr., La Jolla, CA 92093, United States of America
[3] Author to whom correspondence should be addressed.

E-mail: tolley@ucsd.edu

Keywords: bioinspired, suction disc, adhesion

Supplementary material for this article is available online

Abstract

Adhesion is difficult to achieve on rough surfaces both in air and underwater. In nature, the northern clingfish (*Gobiesox maeandricus*) has evolved the impressive ability to adhere onto substrates of various shapes and roughnesses, while subject to strong intertidal surges. The suction disc of the clingfish relies on suction and friction to achieve and maintain adhesion. Inspired by this mechanism of attachment, we designed an artificial suction disc and evaluated its adhesive stress on rough surfaces and non-planar geometries. The artificial suction disc achieved adhesion strengths of 10.1 ± 0.3 kPa in air on surfaces of moderate roughness (grain size, 68 μm), and 14.3 ± 1.5 kPa underwater on coarse surfaces (grain size, 269 μm). By comparison, a commercially available suction cup failed to exhibit any significant adhesion in both scenarios. The roughly 2 g heavy clingfish-inspired suction discs gripped concave surfaces with small radii of curvature (12.5 mm) and supported payloads up to 0.7 kg. We correlated the effect of key bioinspired features (i.e. slits, a soft outer layer, and body geometry) to adhesion performance using contact visualization techniques and finite element analysis (FEA). The suction discs were then tested on a remotely operated vehicle (ROV) to demonstrate their utility in the soft manipulation of fragile objects.

1. Introduction

Non-destructive adhesion (i.e. reversible adhesion that does not damage or alter the substrate) to rough surfaces represents a challenge for robotic systems in both wet and dry environments. Many strategies for attachment in air (e.g. based on van der Waals forces [1, 2]) lose their effectiveness underwater and thus are specific to the type of environment [3]. Previous work has turned to nature to provide inspiration for the design of adhesive systems [4, 5]. Attachment mechanisms employed by organisms have been classified into the categories of mechanical interlocking [6], friction [7], chemical bonding [8, 9], dry adhesion (i.e. van der Waals forces) [1, 10–12], wet adhesion (i.e. capillary adhesion) [13], and suction (driven by a pressure differential) [14, 15]. Interlocking involves the use of structures, such as hooks and claws, to catch onto surface asperities or penetrate a surface [16]. Chemical adhesion involves the use chemical bonds to adhere to surfaces either permanently, such as in mussels [9], or temporarily, as demonstrated in echinoderms such as sea stars [8]. Dry adhesion relies on van der Waals forces between microscopic structures along an adhesive pad and a surface. Adhesion relying on van der Waals forces is commonly used by terrestrial organisms ranging from arthropods such as spiders [12] to reptiles such as geckos [1, 17]. Wet adhesion leverages capillarity to form a liquid bridge between an attachment pad and a substrate [18]. Tree frogs, for instance, leverage wet adhesion by secreting mucus in between channels present on their toe pads to form a capillary meniscus, allowing for attachment to a substrate [13]. Insects employ a similar strategy to adhere to surfaces using an adhesive secretion that originates from the foot pads to take advantage of wet adhesion, as demonstrated in ants and flies [19, 20]. Friction as an attachment mechanism resists movement parallel to a surface [21] and can result from various mechanisms, one

of which includes microscopic interlocking with surface asperities [16]. Lastly, suction is induced by the formation of a pressure differential between the surrounding environment and an adhesive disc [14, 15, 22, 23]. Organisms employ multiple types of these attachment strategies in order to adhere to surfaces.

Each environment type poses its own unique set of challenges to adhesion, resulting in new adaptations of these attachment devices [3]. For instance, an organism in an underwater environment may be subjected to disruption due to buoyancy or variable fluid flow, which would thereby influence the strategy for attachment. As an example, adhesion strategies utilized by organisms in wet environments less commonly employ van der Waals forces for adhesion. However, recent work on tree frogs [13] and abalone [10] suggest their use of van der Waals, in addition to capillarity, to adhere. Aquatic organisms commonly achieve reversible adhesion via suction in coordination with mechanical interlocking or friction [6]. The remora, a symbiotic fish that attaches to sharks, whales, and rays, uses a specialized dorsal suction disc with rigid spines to withstand highly directional flow while secured to the body of its host [22].

Attachment devices observed in nature inspire new adhesive designs in artificial systems as a form of biomimicry [24]. Bioinspired modes of attachment have been applied to the field of robotics [25] to enhance locomotion [26, 27] and manipulation [28, 29]. Robotic footpads composed of gecko-inspired dry adhesives [25] and of spines and hooks [30] have provided robots with the ability to climb dry glass walls and fabric walls, respectively. Similarly, bioinspired, non-destructive adhesion methods are important for the growing field of soft robotics [31], such as for crawling robots that rely on anchoring to aid in elongation and contraction of the body [27].

Bioinspired attachment devices have also been used to enhance robotic manipulation [29]. In dry environments, gecko-inspired adhesives have been applied to soft robotic grippers to enhance their grasp of complex shapes [32] and manipulate large objects in microgravity [33]. Gecko-inspired adhesives have also been used in conjunction with a chamber of controlled subatmospheric pressure to achieve adhesion onto deformable surfaces [34].

Efforts have been made to improve adhesion in wet and damp conditions to enhance locomotion and manipulation. Bioinspired, microstructured adhesives, which have been traditionally used in dry environments, have been modified via chemical coating [35], material composition [36], and geometry [37, 38] to provide adhesion in wet conditions. The octopus has served as a source of inspiration for robotic grippers, including an actuated, soft-body continuum arm to grip around surfaces [39]. The suckers of the octopus have inspired the development of artificial suction cups with varying surface textures made of silicone, which have been tested on smooth surfaces [40]. A remora-inspired suction disc was developed, combining a suction chamber with actuated rigid spines to adhere onto surfaces of roughnesses up to 200 μm [41]. The examples listed above demonstrate the benefits of coupling bioinspired adhesion devices and the fields of materials science and robotics to provide enhanced attachment capabilities both in and out of water. However, further studies should be conducted to improve adhesion capabilities to rough surfaces in water while remaining passive or unactuated.

We sought inspiration from the clingfish to engineer a device to reversibly adhere to rough surfaces underwater. The clingfish (*Gobiesox maeandricus*) lives in intertidal habitats and clings to rocks while subject to continuous wave action of various forces and intensities. Respiration tests have demonstrated that little sustained muscular exertion is required to maintain adhesion [42]. The passive nature by which the clingfish remains adhered to a substrate suggests a biomimetic analog may also need not be actuated to sustain adhesion. The ability of the biological specimen to cling and resist powerful intertidal forces is thanks to a ventral suction disc supported by the pelvic and pectoral girdles [42]. The suction disc functions by establishing a chamber of subatmospheric pressure that is capable of sealing to surface irregularities [43], thereby sustaining pull-off forces that are 80 to 230 times the body weight of the clingfish [44].

The clingfish accomplishes attachment via hierarchical mechanisms of adhesion, or multiple forms of adhesion on both micro- and macroscopic scales. Research has suggested that clingfish adhere by suction and maintain their grip via friction [44]. Capillary adhesion is also considered to play a role in attachment [43, 44]. Other mechanisms may also be at play, such as van der Waals forces, although this mechanism would be diminished in liquids as compared to air assuming a constant gap width. Involvement of van der Waals forces in adhesion may be non-nominal when the fibrils of the papillae are in close proximity to the substrate, a similar phenomenon being reported in tree frogs [13]. For this paper, we chose to investigate the impacts of the clingfish morphology and structure on two primary methods for attachment, via suction and friction.

On the macroscopic scale, the displacement of the surrounding fluid from the concavity of the clingfish disc induces suction by creating a chamber of sub-ambient pressure formed at the intersection of the pelvic and pectoral fins [42–44]. The disc margin, or the perimeter of the suction disc, acts to seal the suction chamber and is critical to the success of the grip of the clingfish. The disc margin is lined by rows of hexagonal pads, or marginal papillae [42], that aid in the sealing of the suction chamber. Previous work describes an extracellular cuticle that is secreted by the papillae [42]. We refer to this extracellular cuticle as 'fibrils' in this work. These structures are hypothesized to play a role in increasing the frictional footprint of the clingfish, thereby conforming to surface asperities and preventing the slip of the disc margin.

Inspired by the ability of the clingfish to resist axial loads, we developed a non-destructive method of attachment that functions on rough and elaborate surfaces without necessitating complex fabrication or controlled actuation. We first investigated the macro- and microscopic structures involved in adhesion of the clingfish using scanning electron microscopy (SEM). We then applied our findings to create artificial clingfish-inspired suction discs. These discs were composed of silicones of varying stiffnesses in specific molded geometries to tailor adhesion performance. The artificial suction discs were then applied to a manipulator of a remotely operated vehicle (ROV) and tested for performance when handling delicate objects, as an example application of the technology.

2. Materials and methods

2.1. Morphology of biological suction disc

In an effort to better understand the underlying mechanisms of attachment of the clingfish, we dissected and imaged the suction disc of both fresh and preserved clingfish specimen. Two live clingfish (*Gobiesox maeandricus)* were collected along the San Diego coastline under a collection permit to accredited organisms' collector, Zerofski from Scripps Institution of Oceanography. Animal care protocol IACUC #S11071 to Deheyn was used for fish euthanasia and fresh tissue was analyzed the day of animal sacrifice. Observations were also performed on preserved clingfish samples obtained from the Scripps Marine Vertebrate Collection. Clingfish were preserved in 70% ethanol and were therefore observed to be devoid of secretions and exhibited tissue dehydration from the preservation process.

Fresh and preserved tissue samples were imaged under brightfield microscopy (Carl Zeiss AG, Germany) using a SMZ1500 Nikon camera. The disc margin of the suction disc of the preserved clingfish was imaged under the Scanning Electron Microscope FEI Apreo SEM (Thermo Fisher Scientific, Inc.).

The brightfield micrographs were analyzed using ImageJ [45] to calculate the area of the disc margin relative to the entire suction disc surface area. The difference in surface areas between the disc margin and the entire suction disc was normalized to the surface area of the entire suction disc. We calculated that the disc margin comprised approximately 65% of the total suction disc footprint. These measurements were then used for the design of biomimetic suction discs.

2.2. Biomimetic suction disc design

We applied two key concepts of suction and friction to avoid slip while sealing the disc margin to create a bioinspired suction disc that successfully adhered onto textured surfaces and irregular shapes (figure 1). The low-pressure chamber of the artificial disc was composed of a silicone of shore hardness 20A, Young's modulus 1.11 MPa [46] (Dragon Skin 20, Smooth-On, Inc.) (figures 2(f) and (g)). The soft fibrils originating from the papillae of the clingfish inspired the use of micropillars to line the disc margin (figures 2(g) and (h)). The dimensions of the synthetic micropillars were chosen to be the same order of magnitude as the biological fibrils. We compared the performance of suction discs with micropillars to that of discs without. For the latter, the soft fibrils of the clingfish were approximated as a thick layer of silicone of shore hardness 00-30, Young's modulus 125 kPa [47] (Ecoflex 00-30, Smooth-On, Inc.) (figure 2(f)). We will refer to the silicone layer lining the disc margin as 'soft' and that of the suction chamber as 'stiff' due to their relative stiffnesses (i.e. 125 kPa versus 1.11 MPa, or about 9× difference in stiffness).

We fabricated and tested a total of six prototypes, two with micropillars and four without, to evaluate the effect of three design parameters (disc geometry, a soft sealing layer, and slits) on adhesion of the disc to various surfaces (figure 3). Disc geometries were either bilaterally symmetric or radially symmetric. The bilaterally symmetric prototype was designed with two slits in the disc margin, analogous to the intersection of the pelvic fin and the posterior margin of the clingfish, described in previous work as a valve [42]. The bilaterally symmetric disc featured a soft layer in its disc margin. All five other prototypes were radially symmetric.

We fabricated two radially symmetric suction discs with micropillars (2 μm square cross-section, height 10 μm, spaced 1.5 μm apart) (figures 2(g) and (h)) [48]. The disc margin overall was 0.8 mm thick. We tested two stiffnesses for the micropillars, changing the material composition of the micropillars to be either soft (125 kPa) or stiff (1.11 MPa) silicone.

We fabricated three radially symmetric suction discs without micropillars in the disc margin (figure 3). One prototype was designed with a soft layer of thickness 2 mm and with four equally spaced, radially symmetric slits, each angled 15° from the radial direction (figure 1(d)). We hypothesized that slits would improve sealing capabilities of the suction disc by providing geometric (in addition to intrinsic material) compliance to an irregular surface. Another prototype featured a 2 mm thick soft layer and did not have slits in the disc margin. We created a control design, referred to as a stiff disc, which was manufactured without slits and without a soft layer. Across all prototypes, the disc margin accounted for about 65% of the total suction disc footprint, congruent with our measurements of the biological specimen. All six types of suction discs created for this study were 25 mm in diameter and with a suction chamber depth of 4 mm. We detached the discs by either subjecting it to a shear force parallel to the attachment surface, or by lifting one side of the disc margin to relieve the subambient pressure within the suction chamber.

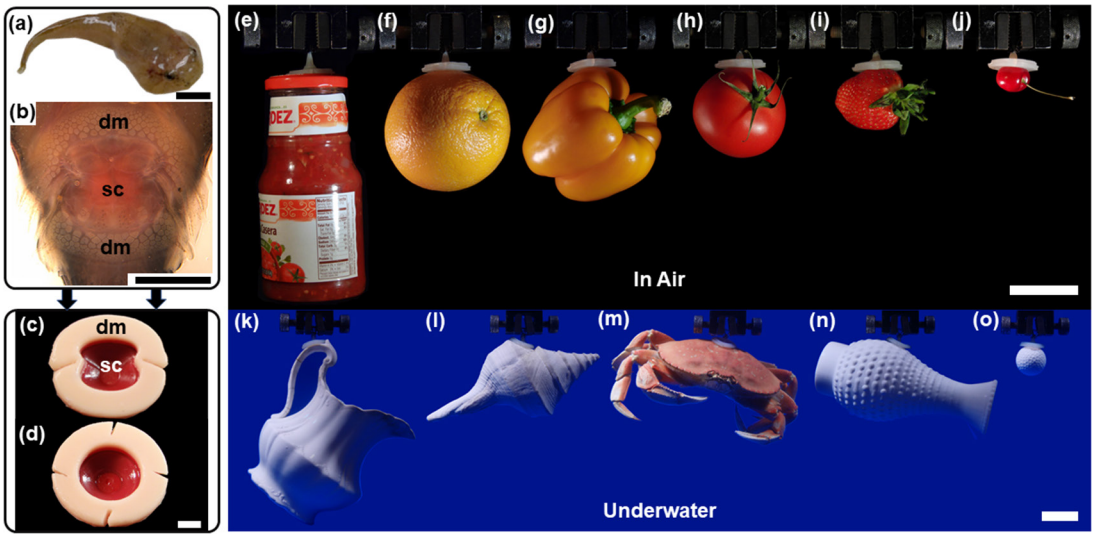

Figure 1. Suction disc clings to highly variable surfaces in air and underwater. (a) Clingfish (*Gobiesox maeandricus*) collected along the coast of Southern California. Scalebar, 10 mm. (b) Ventral view of clingfish suction disc imaged under brightfield microscopy. Disc margin (dm); Suction chamber (sc). Scale bar, 5 mm. (c) Bilaterally symmetric suction disc with two slits. The soft layer of the disc margin (dm) is composed of Ecoflex 00-30. The suction chamber (sc) is composed of Dragon Skin 20. Scale bar, 5 mm. (d) Radially symmetric suction disc with four slits in the disc margin. Scale bar, 5 mm. (e)–(j) Suction disc (radially symmetric, with soft layer, with four slits) adhering to food items in air. Scale bar, 50 mm. (k)–(o) Suction disc (radially symmetric, with soft layer, with four slits) gripping ceramic vase handle, calcareous shell, crab shell, textured vase, and golf ball in water. Scale bar, 50 mm.

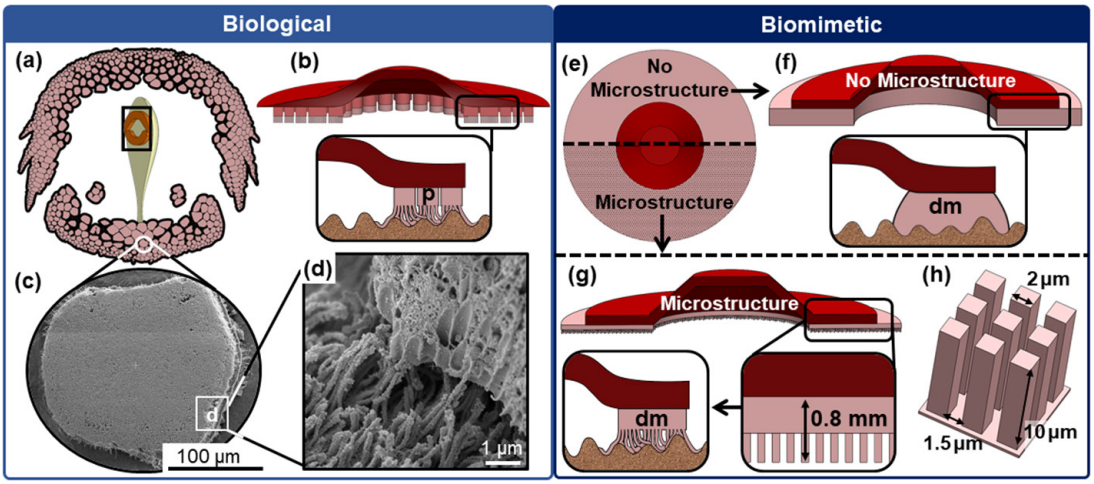

Figure 2. Hierarchical mechanisms of adhesion in clingfish (*Gobiesox maeandricus*) and biomimetic suction discs. (a) Footprint of clingfish disc margin. Generated from brightfield micrographs via image processing, outlining all papillae. Disc margin comprises about 65% of suction disc footprint. Inset: Schematic of ventral suction disc. (b) Schematic of the approximated biological methods of attachment. The pelvic girdle composes the suction chamber. The papilla (p) is represented as cylindrical, with densely packed fibrils that are used to conform to and seal surface asperities. (c) SEM micrograph of single papilla of the disc margin. (d) SEM of isometric view of papilla on fractured edge, fibril shown in lower left. Scale bar, 1 μm. (e) Bottom view of radially symmetric suction discs. (f) Schematic of the suction disc without microstructures. Inset: The soft layer of the disc margin (dm) conforms to surface irregularities. (g) Schematic of a suction disc with micropillars lining the disc margin. Disc margin thickness is 0.8 mm. Inset: Micropillars conform to surface irregularities. Note: microstructure dimensions have been exaggerated for illustrative purposes. (h) Schematic of micropillars of 2 μm square cross-section, height of 10 μm, and spacing of 1.5 μm.

2.2.1. *Fabrication of biomimetic disc*

Artificial suction discs were designed using computer-aided design (Solidworks, Dassault Systems) and fabricated using molds that were manufactured from rigid material (VeroClear, Stratasys Inc.) on a multimaterial 3D printer (Objet350 Connex3, Stratasys Inc.) (figure 4). After printing, the rigid molds were aged in an oven at 40 °C for 4 h to ensure the part fully cured. Body geometries were either circular, or in the bilateral geometry of the clingfish suction disc in accordance to analysis as described in section 2.1. The discs were molded with cylindrical handles 8 mm in diameter, 10 mm in height to provide a gripping surface for a clamp during pull tests.

The suction chamber of each disc was 4 mm in depth, the walls of which were composed of Dragon Skin 20 (Dragon Skin 20, Smooth-On, Inc.) (figure 4). Molds of Dragon Skin were placed in a vacuum

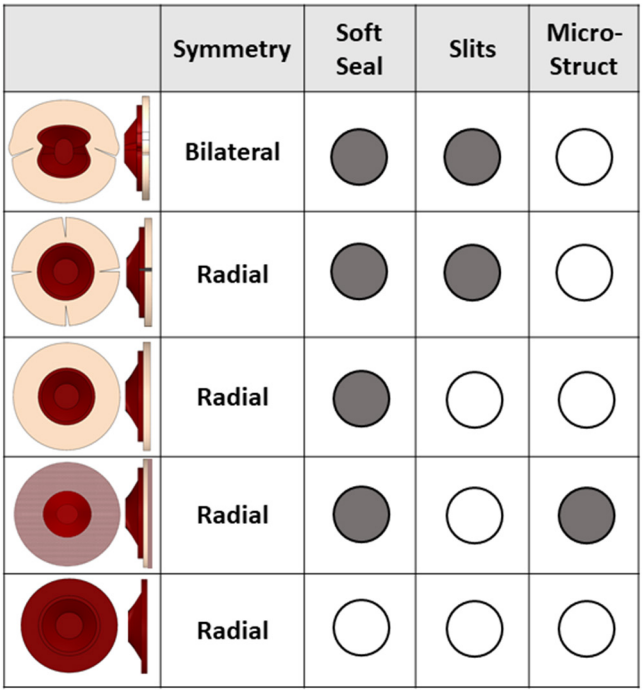

Figure 3. Schematics of different prototype designs. (Row 1) The bilaterally symmetric suction disc was fabricated with slits and a soft layer, without microstructures. (Row 2) A radially symmetric disc was designed with four slits and a soft disc margin, without microstructures. (Row 3) A radially symmetric disc was fabricated with a soft layer, without slits, and without microstructures. (Row 4) A radially symmetric disc was designed with a soft layer, without slits, and with microstructures. (Row 5) The stiff suction disc served as a control for the adhesion experiments. This disc did not have a soft margin, slits, or microstructures.

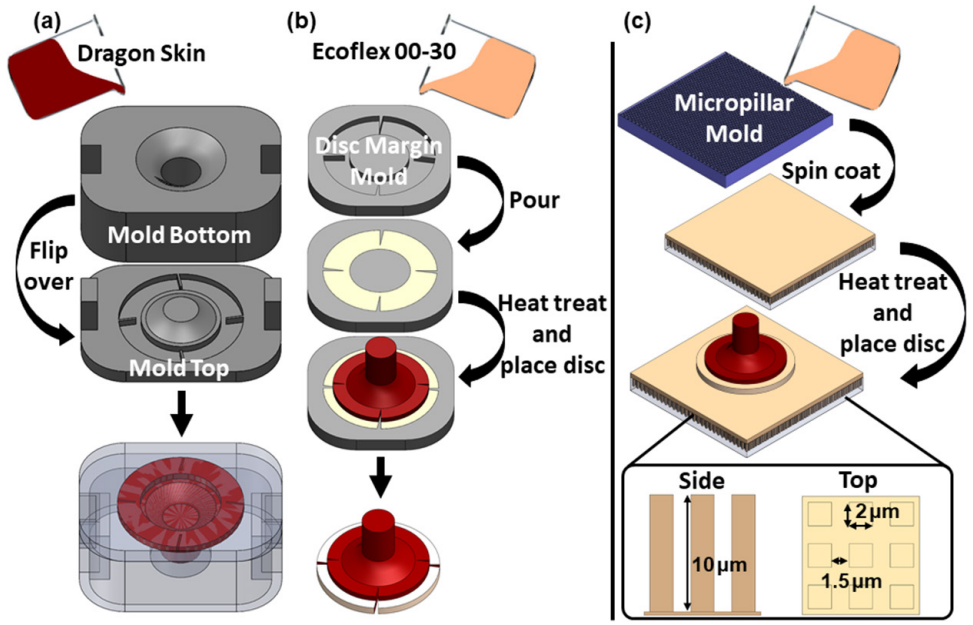

Figure 4. Fabrication process of a suction disc. (a) Stiff backing of the circular, radially slitted suction disc molded with DragonSkin 20 in custom, 3D-printed mold. (b) Soft layer of Ecoflex 00-30 added to stiff, radially symmetric backing in 3D-printed mold. (c) Fabrication of the micropillar array. Spin coat the mold for the micropillar array with silicone elastomer (either Ecoflex 00-30 or Dragon Skin 20). Place the suction disc to be coated in micropillars on heat-treated elastomer. Resulting micropillars are 2 μm squares with a height of 10 μm spaced 1.5 μm apart.

chamber for approximately 5 min to degas the silicone and then fully cured for 1 h 30 min at 40 °C. Samples with a soft layer were coated with a 2 mm layer of Ecoflex 00-30 (Ecoflex 00-30, Smooth-On, Inc.). To apply the soft layer, a mold containing Ecoflex was partially cured at 40 °C for 3 min. The suction chamber composed of Dragon Skin was then added to the partially cured mold of Ecoflex and set to cure for 1 h at 30 °C.

Micropillars were fabricated using a mold provided by NASA Jet Propulsion Laboratory [48] by casting silicone elastomer (Ecoflex 00-30 or Dragon Skin 20) onto a wax mold with the microfeature geometry.

The wax mold and silicone were spun at 800 rpm for 30 s and partially cured (40 °C for 3 min). The remaining layers of the suction disc were then added on to the micropillar layer, and the entire assembly was cured at 40 °C for 15 min.

2.3. Force measurements of biomimetic disc

We evaluated the performance of the suction discs on various surfaces using a mechanical testing system (3342, Instron Inc.; capacity 500 N; and 5965, Instron Inc.; capacity 5000 N) (figures 5(a)–(c)). We then evaluated the performance of a commercially available suction cup (701477, Hillman Inc.; capacity 2.22 N, diameter 25 mm), to provide a comparison to the artificial suction discs. We chose a commercial suction cup with a diameter (and hence contact area) similar to our designs. We secured the suction discs to the mechanical testing setup by means of a clamp and pulled normally from a secured surface. All underwater trials occurred in a bath of tap water, bath depth 20 mm. All pull tests done in air were performed on dry surfaces. Suction discs were preloaded with 2 N, a force sufficient to collapse the chambers and generate subatmospheric pressure within the chambers when released. The load was held for <20 s prior to the start of the pull test. Pull tests were performed with a speed of retraction of 10 mm s^{-1} in triplicate for each substrate type.

To determine the effects of surface roughness on disc performance, experimental surfaces were fabricated with three textures: smooth ($R_a = 0.2$–1.2 μm [49]), moderate (grain size, 68 μm), and coarse (grain size, 269 μm) (figures 5(d)–(f)). The smooth experimental surface was composed of a plate of acrylic. The rough experimental surfaces were fabricated by bonding sandpapers of grain size 269 μm (P60, 3M, Inc.) or grain size 68 μm (P220, 3M, Inc.) to an acrylic plate using an acrylic adhesive (VHB 4905, 3M, Inc.). Experimental textures were replaced between disc trials.

The effect of surface concavity and convexity on disc performance was evaluated on smooth, semi-cylindrical surfaces (halved PVC pipes) of inner diameters: 60 mm, 48 mm, 41 mm, 25 mm, and 15 mm. Outer diameters of the PVC pipes were measured to be 70 mm, 58 mm, 50 mm, 33 mm, and 20 mm, respectively. To test adhesion of the disc to a rough, concave surface, an experimental surface was constructed by bonding sandpaper of grainsize 269 μm to the inner wall of a halved PVC pipe (41 mm diameter) using acrylic adhesive. All experiments involving concave and convex surfaces were performed in triplicate and in a bath of water.

The effect of applying a preload was measured for both smooth and moderate (grain size, 68 μm) surface roughnesses using a mechanical testing system (5965, Instron Inc.; capacity 5000 N). Preloads of 0.5 N, 1.5 N, 2.0 N, 2.5 N, and 3 N were applied to the back of the suction disc prior to being pulled normal to the experimental surface. All trials occurred in a bath of fresh water and in triplicate per preload.

2.4. Longevity of biomimetic disc

We evaluated the longevity of three suction disc types under various loads in air (figures 6(a) and (b)). Longevity tests were performed on (1) a radially symmetric disc with a soft layer and four slits, (2) a radially symmetric disc without slits and without a soft layer, and (3) a commercial suction cup. We pressed the discs to a smooth stone surface, to which we fixed a hook using epoxy. The stone surface was water-worn, of low porosity, and rounded from weathering. Imaging with SEM provided a visual comparison of the stone surface to the experimental surfaces composed of sandpaper used during pull tests (figures S1(a) and (b) (stacks.iop.org/BB/14/066016/mmedia)). We measured the diameters of protruding features on the stone surface to be between 1 and 5 μm. We measured the diameters of local depressions on the stone surface to range between 4 and 10 μm. The weight of the stone and hook totaled 82.5 g. We then increased the total payload every trial by adding brass weights to the hook of the stone. The trials were timed from the moment the loads were applied until the moment of failure, which occurred when the disc dropped the load. Discs remained undisturbed for the length of the trial. Experiments were run in triplicate and monitored via webcam (640 × 360 pixels, frame captured every 20 s; Logitech, Inc.).

2.5. Contact area measurement

We measured the contact area of the disc to a surface using Frustrated Total Internal Reflection (FTIR). The setup for FTIR experiments was custom-built [50] (figures 6(c) and (d)). The station was constructed with a 3D printed mount, 9.7 mm thick acrylic, and natural white LEDs (3528-24VDC, Super Bright LEDs, Inc.). The light emitted from the diodes was internally reflected within the acrylic. The acrylic was wetted with water during wet trials. To visualize the contact area, the suction discs were dyed black using silicone pigment (Silc Pig, Smooth-On, Inc.) during the molding process. Contact with the acrylic plate allowed light to escape from the surface of the acrylic, which was then imaged with a camera (1280 × 780 pixels, 140 pixels cm^{-1}, 40 frames per second; EXILIM EX-FH25, Casio Computer Co., Ltd.).

The discs were either pushed or pulled from the imaging surface. Loads were applied by brass weights to the backing of the suction disc. A load of 0.05 kg applied to the back of a disc generated a force of 0.49 N to push the disc to the imaging surface. A load of 0.2 kg applied to the back of the disc generated a force of 1.96 N to pull the disc from the imaging surface. Discs were then pulled manually to the point of failure (POF). We considered the last frame of the suction disc in contact with the imaging surface to be the POF.

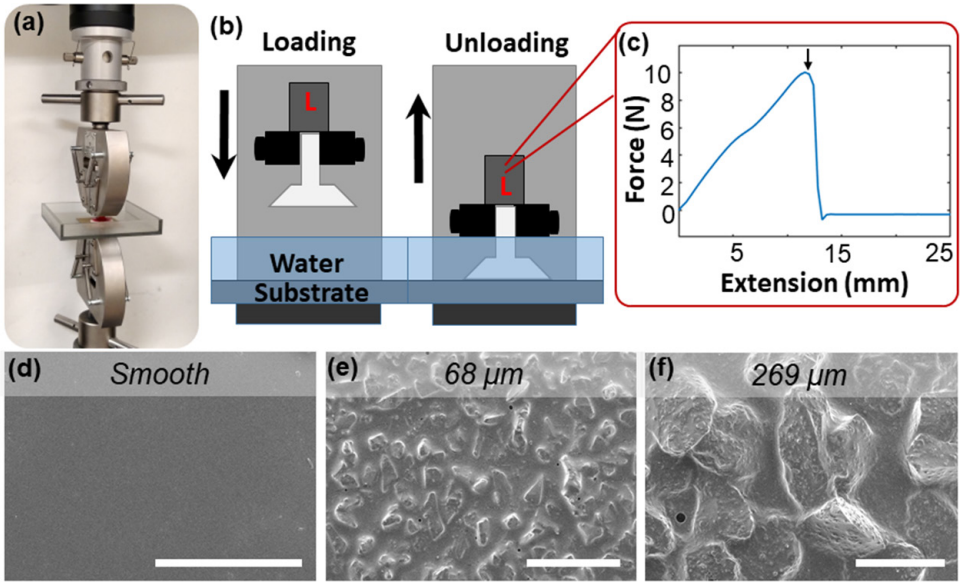

Figure 5. Schematic depiction of adhesive force measurements using a mechanical testing system. (a) Suction discs were secured in a clamp of a mechanical testing machine and engaged with a surface under a preload of 2 N. (b) Illustration of the loading and unloading of the suction disc. The force and displacement were recorded and used to calculate adhesive stress. Experimental surfaces were submerged in a bath of water for all underwater trials. (c) An example plot of force (N) and extension (mm) for the radially symmetric disc with a soft layer in disc margin. Arrow indicates maximum pull-off force achieved by the disc. (d) SEM micrograph of smooth experimental surface, scale bar 500 μm. (e) SEM micrograph of moderately rough (grain size, 68 μm) experimental surface, scale bar 500 μm. (f) SEM micrograph of coarse (grain size, 269 μm) experimental surface, scale bar 500 μm.

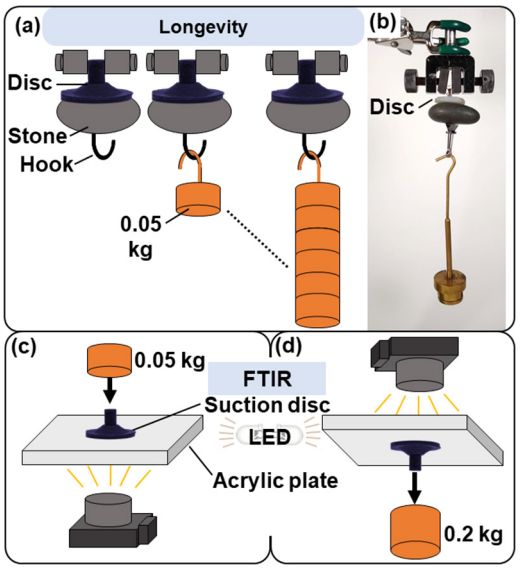

Figure 6. Schematics of experimental setups for longevity and Frustrated Total Internal Reflection (FTIR). (a) Schematic of the experimental setup for the longevity study. A suction disc (radial geometry, with soft layer and slits, without microstructures) adhered to a stone, and brass weights were added per trial to a hook attachment to increase the payload. Trials were timed and the payloads ranged between 0.82 kg to 0.482 kg. (b) Image of a suction disc adhered to the experimental payload (total weight in image: 0.282 kg). (c) Schematic of experimental setup for FTIR; the suction disc adhered to the imaging surface when a brass weight (0.05 kg) was applied to the back of the disc, resulting in a pushing force of 0.49 N. Imaged from below. (d) Schematic of second FTIR experimental setup in which a brass weight of 0.2 kg was used to pull the suction disc from the imaging surface, resulting in a pulling force of −1.96 N. Imaged from above.

The images from FTIR were post-processed by increasing the contrast by 100% and sharpness by 10% and reducing the brightness by 20%. The color temperature of the image was also set to 1500 K. The original images are provided in the supplemental materials (figure S2).

2.6. Finite element analysis (FEA) of disc

To understand the effect of incorporating slits in the disc margin on the total strain energy and stress distribution, we performed FEA on two disc types, one with and one without radial slits (both without a soft layer). We measured the equivalent stress and total strain energy of the system subject to a constant vertical compression of 2 mm (figure S3(a)). We selected the vertical displacement to be 2 mm, or half the height of the suction chamber, suggesting that the deformation simulated in FEA would be analogous to evacuating half of the suction chamber to engage with a surface.

FEA was conducted and analyzed using ANSYS 19.2. We experimentally determined the material properties of DragonSkin 20 by performing a tensile test using a mechanical testing setup (3342, Instron Inc.). The data was best fit to the Yeoh 3rd order hyper-elastic model. Parameters for the model (C10, C20, C30, D1, D2, D3) were 99 161 Pa, −1604 Pa, 1065.2 Pa, 0 Pa^{-1}, 0 Pa^{-1}, and 0 Pa^{-1}, respectively.

We used 20-node Brick elements to mesh the suction disc model (figure S3(b)). The FE model had 2698 and 2634 elements for the case with slits and without slits, respectively. Element shapes with an aspect ratio

close to one are highly desirable in FE analysis for better accuracy and convergence. In our FE model for all cases, more than 60% of the total elements had an aspect ratio between one to two. The average aspect ratio of the elements was 2.87 ± 1.08, while the average skewness was 0.194 ± 0.14.

Due to radial symmetry of the design, we chose to model a quarter of the suction disc in FEA to reduce time required for computation (figure S3(c)). The total strain energy of the quadrant was multiplied by 4 to represent the entire disc. We did not account for surface energy, friction, or vacuum and neglected the contribution of a soft layer in the simulation. We varied one boundary condition of constraining deformation of the disc margin in the axial direction. The surface was assumed to be frictionless. A constant, 2 mm displacement in the axial direction was imparted on the back of the suction chamber. We compared the results for deformation, Von-Mises stress, and elastic energy from each case.

3. Results

3.1. Adhesion mechanisms of the clingfish suction disc

The clingfish has an impressive grip when subject to normal loads, yet the same is not true for tangential forces. Manipulations of a euthanized clingfish demonstrated that the suction disc does not resist shear motion when moved across a glass slide using dissection forceps (movie S1). However, when pulled perpendicular to the surface of the glass slide, the euthanized clingfish resisted the axial load, thereby causing the glass slide to lift from the benchtop. Using image processing of brightfield micrographs of the suction disc of a clingfish, we calculated that the disc margin accounts for about 65% of the total suction disc footprint of the clingfish (figure 2(a)).

When a fractured edge of a papilla was imaged under SEM, one can observe that densely-packed, presumably soft fibrils emanate from channels (0.25 μm diameter, at a spacing of 0.02 μm) (figure 2(d)). Fibrils shown in SEM micrographs lack a consistent orientation, contrary to other adhesive structures seen in nature for other organisms, such as the directional setae of the gecko [1, 17].

The soft fibrils increase the frictional footprint of the clingfish by conforming to surface asperities. By doing so, the fibrils resist an inward slip of the disc margin and seal the suction chamber. Suction and friction are two methods of attachment that act in combination to successfully adhere the clingfish to rough substrates (figure 2(b)).

3.2. Performance of the micropillars

We compared the effect of micropillars and their stiffness on the adhesive capabilities of the suction disc to flat, rough surfaces both in air and underwater. To quantify the effect on adhesion, we measured the maximum adhesive stress (σ; $\sigma = F_{ad}/A$, where F_{ad} represents the maximum pull-off force, and A represents the surface area of the biomimetic disc) to evaluate adhesion of the suction disc on three types of surface roughnesses—smooth (R_a = 0.2–1.2 μm [49]), moderate (grain size, 68 μm), and coarse (grain size, 269 μm).

In air and underwater, the best performing suction disc with microstructures was covered with soft micropillars (12.4 ± 1.1 kPa smooth, 11.4 ± 0.7 kPa moderate, 5.5 ± 0.1 kPa coarse, wet; 10.4 ± 0.1 kPa smooth, 9.9 ± 0.1 kPa moderate, dry) (figures 7(a) and (b)). Suction discs with micropillars composed of the stiffer silicone failed to adhere to the dry surfaces, regardless of surface roughness. Additionally, on submerged surfaces of a coarse roughness, the suction discs with soft micropillars were capable of adhering to the testing surface whereas those with stiff micropillars were not.

We imaged the micropillars and observed how they behaved when subject to load. We pressed a glass slide atop the micropillars to observe their deformation. The micropillars composed of stiffer silicone deformed less when subject to a compressive and shear load (figures 7(e) and (f)). The micropillars composed of softer silicone were visibly able to bend and fold to the glass slide (figures 7(g) and (h)). When a shear load was not applied, the micropillars of soft silicone would clump and bundle. We concluded that the pillars of soft silicone intermeshed together to better seal the perimeter, in comparison to the pillars of stiff silicone.

However, for moderate and coarse surfaces in water, the best performing suction discs with soft micropillars performed 1.3 and 2.4 times worse, respectively, in comparison to the suction disc without micropillars (figures 7(a) and (b)). Thus, we found that for both of these designs, the microstructures reduced the performance of the suction disc when compared to its analog without microstructures.

3.3. Adhesion without micropillars to rough substrates

Using suction discs without micropillars, we evaluated the effect of body geometry and slits on how they impact adhesion to rough surfaces. All three clingfish-inspired suction discs with a soft silicone disc margin outperformed commercial suction cups on rough surfaces both in and out of the water. In air, the biomimetic disc supported dynamic loads up to roughly 305 times its weight (2.3 g disc; 0.7 kg load, brass weights) (figure S4 and movie S2).

On flat, rough underwater surfaces, the circular suction disc with radial slits and a soft layer outperformed all other prototypes and a commercially available suction cup (movie S3). In our underwater trials, this top-performing suction disc achieved adhesive stresses of 13.7 ± 0.4 kPa (smooth), 18.3 ± 0.4 kPa (moderate), and 14.3 ± 1.4 kPa (coarse) (figure 8(a)). By comparison, while the commercially available suction cup achieved a high adhesive stress on smooth

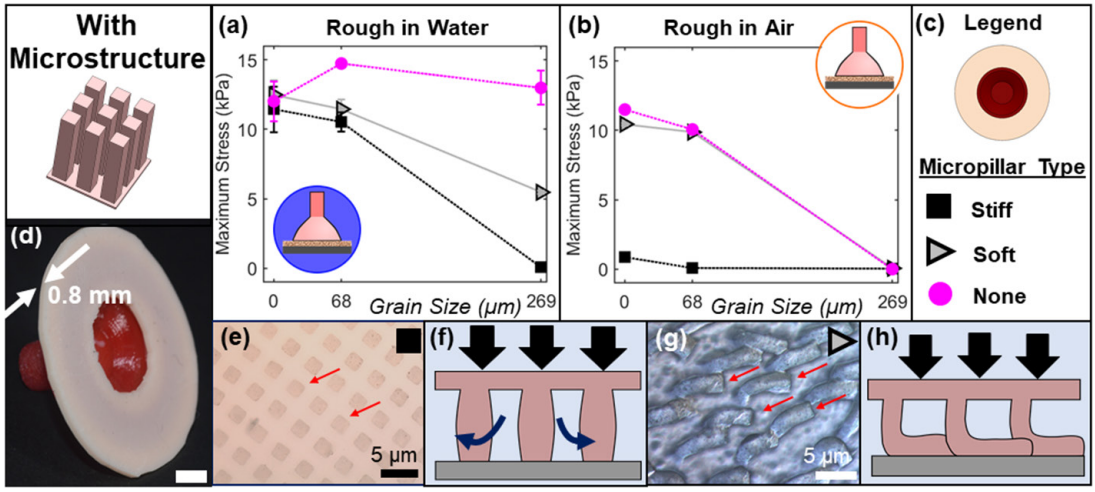

Figure 7. Maximum adhesive stress for discs with micropillars on rough surfaces. (a) Discs with micropillars, average ($n = 3$; ±Std Dev) maximum adhesive stress across flat surfaces of roughnesses: 0 μm, 68 μm, and 269 μm, in water. (b) Discs with micropillars, average maximum adhesive stress across flat, rough surfaces in air. (c) Legend containing schematic of prototype body geometry (radially symmetric, with a soft layer, without slits). Prototypes vary by presence and material stiffness of micropillars. Disc with micropillars composed of stiff silicone, dark square. Disc with micropillars composed of soft silicone, grey triangle. Disc without micropillars, pink circle. (d) Image of a suction disc with a layer of micropillars; arrows indicate the disc margin thickness, which was measured to be 0.8 mm. Scale bar, 5 mm. (e) Brightfield micrograph of top view of micropillars composed of stiff silicone, subject to a glass slide sheared parallel to the surface. Arrows indicate individual micropillars, shown with a square cross-section. (f) Illustration of stiff micropillars allowing fluid to pass between columns. Vertical arrows illustrate a force exerted on the micropillars. Curved arrows illustrate the passage of fluid in between micropillars. (g) Brightfield micrograph of top view of micropillars composed of soft silicone, subject to shear force. Arrows indicate individual micropillars, which bend when subject to external force. (h) Illustration of soft micropillars deforming and intermeshing when subject to a load. Load indicated by vertical arrows.

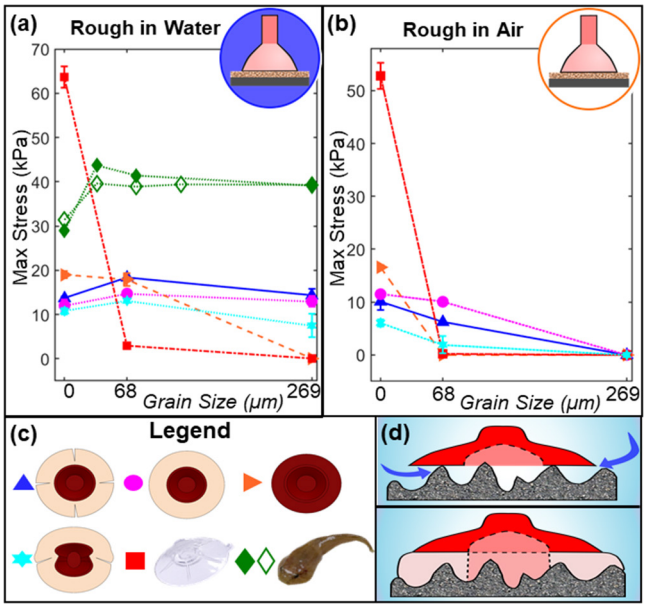

Figure 8. Adhesion to rough surfaces of discs without micropillars. (a) Disc without micropillars, average ($n = 3$; ±Std Dev) maximum adhesive stress across flat, rough surfaces in water. (b) Disc without micropillars, average maximum adhesive stress across flat, rough surfaces in air. (c) Legend containing schematics of prototypes (bottom view) and their corresponding symbol within the adhesive stress curves. Soft layer of Ecoflex (light colored), stiff silicone backing of suction chamber (dark colored). Suction disc variants (no micropillars): radially symmetric with four slits and soft layer (blue triangle); radially symmetric with soft layer and without slits (pink circle); radially symmetric with stiff disc margin (orange triangle); Bilaterally symmetric with soft layer (light blue star); Commercially available suction cup (red square). Clingfish adhesive stress, median values shown, data from Wainwright *et al*. 2013 [44] (solid green diamond), data from Ditsche *et al* [43] (white diamond). (d) Schematic of the effects of the soft layer in the disc margin on sealing to surface irregularities. Stiff backing (dark colored), soft silicone (light colored).

surfaces (63.6 ± 2.3 kPa), it performed poorly on rough surfaces, reaching 2.8 ± 0.3 kPa on a moderate roughness. The commercial suction cup failed to adhere to the coarse surface.

Conversely, in air, a circular disc with a soft layer and without slits outperformed (10.1 ± 0.2 kPa) all other prototypes and a commercially available suction cup on dry surfaces of a moderate roughness (figure 8(b)).

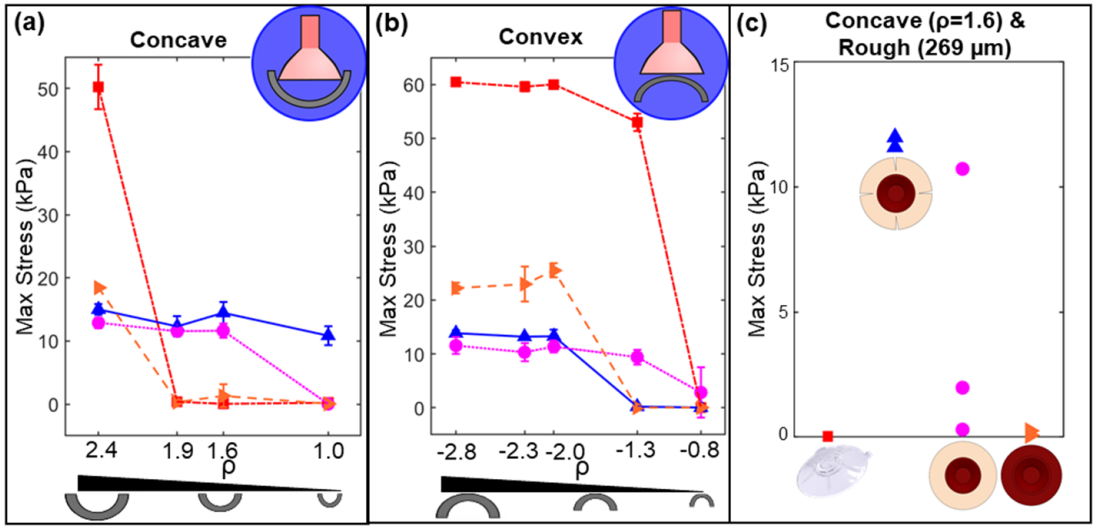

Figure 9. Adhesion to irregular shapes of discs without micropillars. (a) Disc without micropillars, average ($n = 3$; ±Std Dev) maximum adhesive stress across concave surfaces, underwater. Concavity represented as the dimensionless ratio (ρ) of radius of curvature of the surface to the radius of suction disc. Suction disc variants (no micropillars): radially symmetric with four slits and soft layer (blue triangle); Radially symmetric with soft layer and without slits (pink circle); radially symmetric with stiff disc margin (orange triangle); commercially available suction cup (red square). (b) Disc without micropillars, average maximum adhesive stress across convex surfaces, underwater. (c) Adhesive stress of suction discs to a rough (grain size, 269 μm), concave ($\rho = 1.6$) surface, underwater. Three trials were performed per disc type.

Despite being the top performing design in the underwater trials, the disc with slits showed weaker adhesion in the dry trials, with a roughly 1.6 times decreased (6.2 ± 0.2 kPa) suction ability as compared to the discs with a continuous soft layer. The commercial suction cup failed to adhere to both moderate and coarse surfaces in air. All the suction discs tested failed to adhere to coarse surfaces in air.

The disc geometry affected adhesion capabilities in both wet and dry trials; the radially symmetric disc geometry achieved adhesive stresses about 1.9 times stronger underwater and about 5.2 times stronger in air than the bilaterally symmetric disc on rough surfaces.

The presence of a soft layer in the disc margin improved adhesion capabilities in both wet and dry trials. To understand this effect, we compared the performance of the circular suction discs, both without slits and with and without a soft layer. The stiff disc achieved higher adhesive stresses on smooth surfaces (18.9 ± 0.8 kPa, wet; 16.6 ± 0.4 kPa, dry), in comparison to the disc with a soft layer (12.0 ± 1.4kPa, wet; 11.5 ± 0.2 kPa, dry). However, while a stiff disc margin enhanced performance on smooth surfaces, it compromised performance on textured surfaces. For instance, the prototype with a soft layer in the disc margin achieved an adhesive stress of 13.0 ± 1.2 kPa on a coarse surface underwater, while the prototype with a stiff disc margin failed to adhere. The stiff disc performed 6.4 times better than the commercial suction cup at a moderate surface roughness under water, as the material of the stiff suction disc was still more compliant than the commercial suction cup. Thus, the stiffer the material in contact with a surface, the less effectively it can conform to irregularities and maintain the suction chamber sealed (figure 8(d)).

3.4. Adhesion to irregular shapes

Much like the intersection of the pelvic and pectoral fins of the clingfish, slits in the disc margin of the biomimetic discs provided a geometric compliance to the body. Slits thereby impacted the adhesive performance of the disc to irregular shapes. We measured adhesive stress of the disc to concave and convex surfaces, normalizing the radius of curvature of the surface by the radius of the suction disc (ρ; $\rho = R_{surface}/R_{disc}$, where $R_{surface}$ represents the radius of curvature of the surface, and R_{disc} represents the radius of the suction disc). To understand the effect of slits on adhesion to irregular surfaces, we performed experiments on only the radially symmetric suction discs, which removed the effect of body geometry on adhesive performance.

The artificial suction disc with four slits and a soft layer outperformed all other prototypes and the commercial suction cup on concave surfaces with small radii of curvature ($\rho < 1.9$) (figure 9(a)). The disc with slits performed consistently across all tested concavities, with an average adhesive stress of 13.2 ± 1.9 kPa across all four surfaces. Slits improved performance about 1.24 times on moderate ($\rho = 1.6$) surface concavities. Slits coupled with a soft layer in the disc margin adhered to the smallest surface concavity ($\rho = 1.0$) (movie S4), with an adhesive stress of 10.9 ± 1.5 kPa, while all other disc prototypes and the commercial suction cup failed to adhere. All suction discs were unable to adhere to a surface concavity of $\rho = 0.6$, as the suction discs were too large for the radius of curvature and

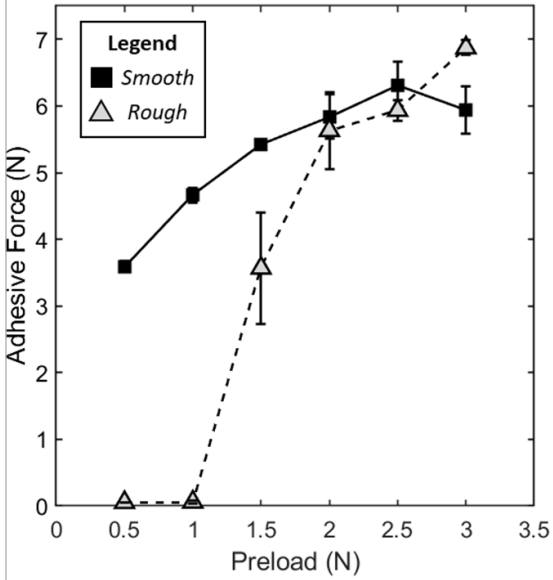

Figure 10. Adhesive force based on preload and surface roughness. Average ($n = 3$; ±Std Dev) force of adhesion of a disc (radially symmetric, soft layer, no slits, no microstructures) for a range of preloads. Trials performed on a smooth surface represented as dark squares. Trials performed on a rough surface (grain size, 68 μm) represented as light triangles.

were physically unable to fit within the pipe to create a sealed chamber of subambient pressure. Overall, we observed that slits provided a geometric compliance that resulted in the capability to better conform and seal to concave surfaces.

We also observed that the soft layer in the disc margin aided in adhesion to concave surfaces. The soft silicone layer yielded adhesion strengths of 11.6 ± 0.6 kPa ($\rho = 1.9$) and 11.7 ± 1.2 kPa ($\rho = 1.6$), greatly outperforming the disc with a stiff disc margin, which failed to adhere to the moderate surface concavities. The stiff suction disc and commercial cup both lost all adhesive capabilities, at moderate concavities ($\rho = 1.6$). We therefore concluded that the soft silicone filled gaps between the suction chamber and concave surface, improving adhesion performance.

We observed that the soft layer in the disc margin reduced adhesive capabilities of the suction disc to convex surfaces for all but the smallest radii of curvature ($|\rho| < 1.3$) (figure 9(b)). Slits also reduced adhesion to convex surfaces with a small radius of curvature, observed when comparing the performance of discs with and without slits (0.2 ± 0.2 kPa, 9.4 ± 1.4 kPa, respectively; $\rho = -1.3$). The stiffness of the disc margin was observed to be most influential to adhesive strength for discs on convex surfaces. The commercial suction cup and stiff suction disc were able to withstand greater pull off forces on larger surface convexities ($|\rho| > 2.0$) in comparison to the discs with a soft disc margin. A threshold convexity, or a convexity at which the discs failed to adhere, was observed as an abrupt decrease in performance, occurring at moderate convexities ($\rho = -2.0$) for the radial disc with slits and for the disc without a soft layer, and at higher convexities for the commercial suction cup ($\rho = -0.8$).

Coupling concavity and surface roughness, we tested adhesion of the disc to a rough (grain size, 269 μm), concave ($\rho = 1.6$) surface (figure 9(c)). The radial suction disc with a soft layer and slits (no microstructures) achieved consistently higher adhesive stresses (averaged to 11.7 ± 0.2 kPa) in comparison to the commercial suction cup and the suction discs without slits (one with and one without a soft layer). The stiff discs were unable to adhere across the trials. The disc with a soft layer and without slits was less consistent in its performance, achieving adhesive stresses ranging from 0.3 kPa to 10.7 kPa. We attribute part of the inconsistent performance to the absence of slits from the disc with a soft layer, suggesting that the disc was less able to radially expand when pressed to the surface due to the rough texture. The disc without slits would therefore be less able to fill the gaps caused by the concave surface due to the rough texture. The consistency and high adhesive stresses resulting from the disc with a soft margin and slits led us to conclude that this design performed best for rough, concave surfaces in comparison to all other prototype designs.

3.5. Effect of preload on adhesive performance

A minimum preload was required to initiate attachment of the suction disc to experimental surfaces. To smooth surfaces, preloads of 0.5 N were capable of initiating attachment and resisting 3.6 ± 0.1 N of pull of force until separation from the surface (figure 10(a)). However, the adhesive performance of the suction disc seemed to stabilize around 5.8 ± 0.3 N given a preload of 2 N. Conversely, for moderately rough surfaces (grain size, 68 μm), a minimum preload of 1.5 N was required to attach the disc to the experimental surface, generating an adhesive force of 3.6 ± 0.8 N (figure 10(b)). Applying a preload of 1.5 N yielded an inconsistent adhesive performance, resulting in an inability to adhere to the moderately rough experimental surface in some instances. Increasing the preload to 2 N increased the adhesive force of the suction disc to 5.6 ± 0.6 N, and allowed for reliable and consistent adhesion to the experimental surfaces. Overall, the minimum preload required for attachment of the suction disc was higher for rougher surfaces.

3.6. Longevity of biomimetic disc

We performed longevity tests on (1) a suction disc with a soft layer and four slits, (2) on a suction disc without a soft layer, and (3) on a commercial suction cup. The suction disc with a soft layer and four slits greatly outperformed the suction disc without a soft layer and the commercial suction cup (figure 11). The suction disc without a soft layer was unable to support any of the tested payloads. The commercial suction cup was consistently able to attach to the payloads for only about 1 s across all trials and payloads. The successful

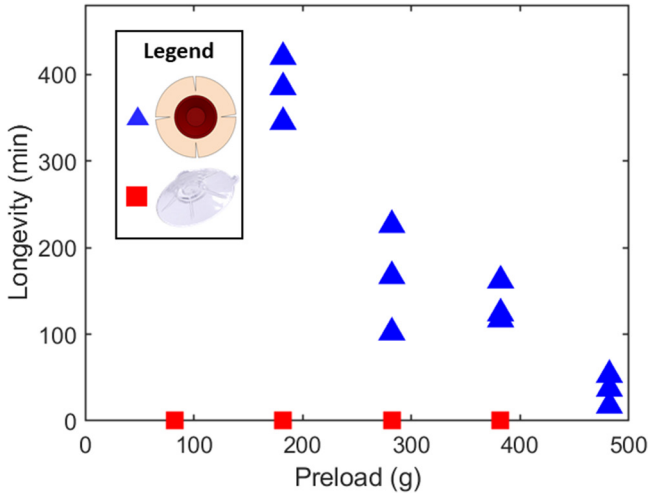

Figure 11. Longevity of a disc bearing a payload. Timed trials of longevity (minutes) of suction discs supporting a payload (g). The results shown in the plot were for the radially symmetric disc with four slits and soft layer (blue triangle) and the commercially available suction cup (red square). The radially symmetric disc without a soft layer was also tested but unable to adhere.

suction disc (radially symmetric with a soft layer, without microstructures, without slits) was successful at attaching to all payloads tested. Payloads of 182 g, 282 g, 382 g, and 482 g were supported for an average time of 383 ± 38 min, 165 ± 62 min, 134 ± 24 min, and 35 ± 18 min, respectively, by the suction disc with a soft layer and four radial slits. Therefore, the suction disc with a soft layer and slits was capable of maintaining adhesion for a significantly longer duration of time, in comparison to the stiff suction disc and the commercial suction cup.

3.7. Visualizing surface contact of discs

We used a contact imaging technique based on Frustrated Total Internal Reflection (FTIR) to visualize how the different suction disc designs interacted with a wet surface when subject to external loads during adhesion. All suction discs used in FTIR did not have micropillars lining the margin. For each load, we measured the area of the disc margin in contact with the imaging surface and normalized it to the total surface area of the suction disc of the reference image.

A stiff disc margin resulted in a low effective area of contact to the wetted imaging surface (figure 12, third row from the top). When applying a load of 0.05 kg to adhere the stiff disc to the imaging surface, the outer margin of the disc raised off the surface, resulting in an inverted configuration (figure 14(c)), and significantly reducing the area in contact with the imaging surface (down to 12% of the total area under the disc, from 59% in the unloaded state). When pulling on the adhesive disc without a soft layer with a load of 0.2 kg normal to the imaging surface, the disc reverted from the inverted configuration, but maintained a small footprint (figure 12, third row from the top). The area in contact remained at 8% but then shifted radially to the outer perimeter when the disc was pulled to failure. As a result, the stiff adhesive disc without a soft layer had about 4.5 times smaller effective contact area at the moment prior to failure, in comparison to those with a soft layer. Furthermore, the commercial suction cup also maintained a small area of contact, ranging from 15% at rest to 10% at the moment prior to failure (figure 12, bottom row). Thus, in general a stiffer material resulted in a smaller effective area of contact with the imaging surface.

Conversely, the disc with a soft layer had a larger contact footprint both when pushed to and pulled from the wetted surface. The disc margin of the prototype without slits and with a soft layer remained in full contact with the imaging surface when pushed and only experienced a 5% reduction in contact when pulled (−1.96 N; figure 12, second row from the top). At the moment prior to failure, we observed that about 36% of the disc margin remained in contact with the surface. The soft layer provided a relatively larger effective area of contact with the imaging surface, thereby increasing the frictional footprint of the biomimetic disc.

The presence of slits also affected the disc footprint during adhesion. The outer perimeter of the disc with slits lifted when the disc was pushed onto the wet imaging surface (figure 12, top row). When pulled from the surface, the disc margin changed from this flared state with a discontinuous perimeter to a closed, continuous perimeter. We hypothesize that the transition between discontinuous to continuous disc margin provides the opportunity to 'regrip' surfaces when pulled. Additionally, when a 0.2 kg load was applied, the percentage of the total area under the disc in contact with the surface reduced by roughly 33% in comparison to its reference. By contrast, the disc without slits only experienced a <5% reduction in contact area.

We compared the surface contact of one disc (with a soft layer, without slits) on dry and wetted imaging surfaces (figure 13). The disc was pulled with a force of -1.96 N in both cases. On a wet imaging surface, the perimeter of the suction disc remained circular. On a

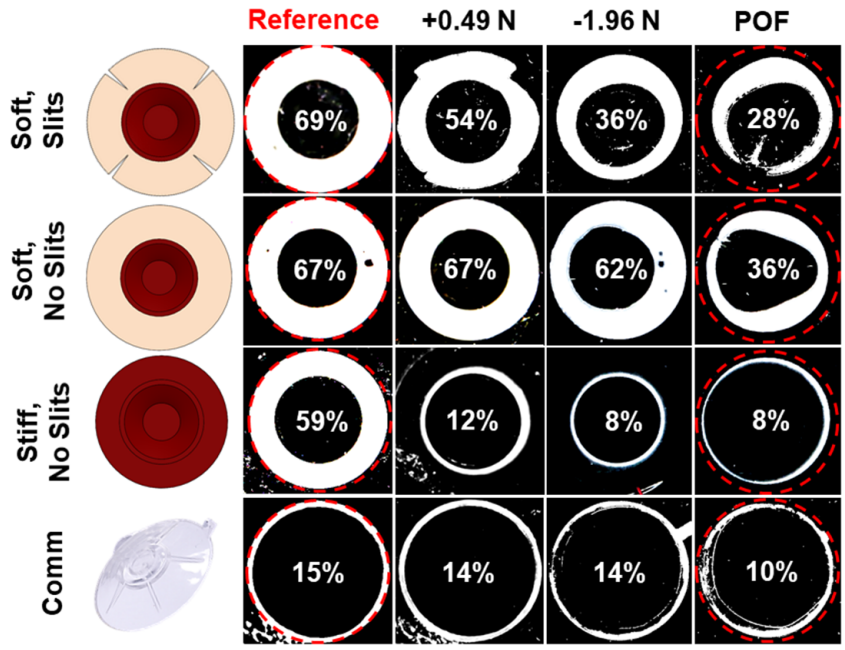

Figure 12. Representative FTIR images of disc footprint. Disc at rest ('Reference') when placed upon the wetted imaging surface. A load (0.05 kg) was applied to push the disc to the imaging surface ('+0.49 N'). A load (0.2 kg) was applied to pull the disc from the imaging surface ('−1.96 N'). The point of failure (POF) was the moment prior to failure of the disc. The dashed circular lines in POF represent the initial size of the disc in the reference state. The percentages are calculated from the area of contact of the disc per load normalized to the total disc area measured in the reference frame. FTIR used to evaluate footprints of three radially symmetric discs and commercial suction cup ('Comm').

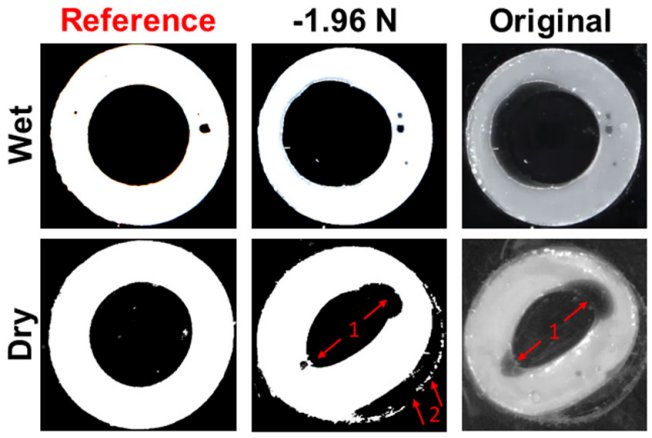

Figure 13. Surface contact of a disc on wet and dry surfaces. Disc (with soft layer, without slits) at rest ('Reference') when placed upon the imaging surface. A load was applied to pull the disc from the imaging surface ('−1.96 N'). Surface contact visualized with FTIR. Original, preprocessed image shown for the disc loaded with −1.96 N ('Original'). (Row 1) Surface contact of the suction disc on a wet surface. (row 2) Surface contact of the disc on a dry surface. Arrows distinguish (1) a cavity formed inside of the suction disc, and (2) residue from the silicone denoting the original footprint of the disc margin prior to loading.

dry imaging surface, the disc elongated to an ellipse. We concluded that this elongation was caused by the anchoring of the disc margin to the dry acrylic plate. In the process of elongation, a cavity was formed along the major axis of the ellipse. The elongation of the disc would result in the propagation of the cavity which could inevitably compromise the seal of the disc. We concluded that the suction disc on a wet surface was better able to prevent elongation due to the presence of a thin fluid film between the disc and the imaging surface.

3.8. Modeling geometric compliance

FEA on two disc types, one with and one without radial slits (both without a soft layer), provided insight on how incorporating slits in the disc margin affected stress and strain energy of the total system. We measured the equivalent stress and total strain energy of the system subject to a constant vertical compression of 2 mm representing the displacement applied to engage the adhesive disc (figures 14(a) and (b)). The total strain energy is the mechanical energy that is stored reversibly within the elastic material [51].

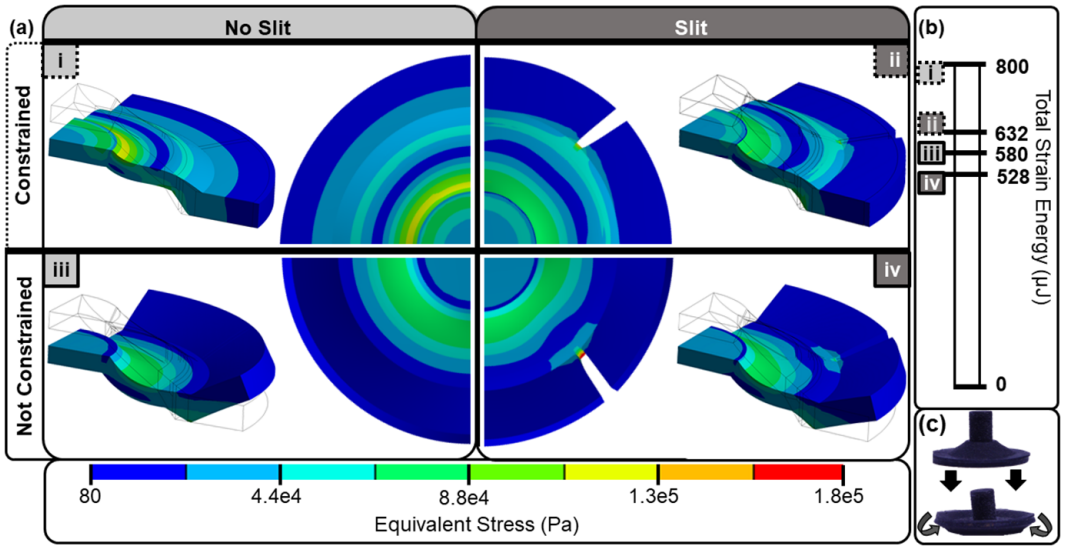

Figure 14. FEA to understand disc behavior when subject to vertical compression. ((a(i) and (ii)) Simulation of equivalent stress (Pa). Axial displacement of disc margin was constrained in simulation for no slit and slit conditions, respectively. (iii) and (iv) Representation of equivalent stress (Pa). Axial displacement of disc margin was unconstrained for no slit and slit conditions, respectively. Scale bar consistent. (b) Total strain energy (μJ) calculated per trial. (c) Demonstration of the outer perimeter of the suction disc lifting from a surface, resulting in an inverted configuration.

A greater total strain energy stored within the body corresponds to higher internal stresses that attempt to restore the original shape. We assume that the primary effect of these stresses during compression onto a flat surface is to resist the compression, which negatively impacts adhesion. Thus, these predictive models allow us to better understand the impact of design parameters on the total strain energy of a system, which affects the adhesive performance of a disc when subject to deformation.

For the simulation, we only considered the effects of deformation to the stiff backing, as the structural integrity of the stiff suction chamber significantly influenced the ability to maintain subambient pressure within the disc. We axially constrained deformation of the disc margin in two of the four simulations. By constraining the disc, we modeled the elastic energy that was stored within the system due to deformation. As modeled under the condition of constrained axial deformation at the disc margin, the total strain energy of the disc with slits (632 μJ) was lower than that of the disc without (800 μJ), when subject to vertical compression (figure 14(b)).

In the simulation that allowed for axial displacement in the perimeter of the disc, it lifted, congruent with what was observed in experimental trials (figure 14(c)). The disc without slits experienced about a 28% reduction in total strain energy and 42% reduction in maximum equivalent stress between constrained and unconstrained boundary conditions. The disc with slits, by contrast, experienced about a 17% reduction in total strain energy and a 17% increase in maximum stress between constrained and unconstrained conditions. The lifted configuration expanded the slits, thereby increasing local stress at the separation node within the disc margin.

3.9. Application to amphibious manipulation

We demonstrated that the suction discs can be successfully applied to robotic manipulation. We focused our efforts to adhering to delicate specimen, such as fresh produce (figures 1(e)–(j) and (k)–(o)), and to enhancing the capabilities of currently existing manipulators, such as those employed by ROVs (figure 15). These applications suggest that the capabilities of the bioinspired disc could extend across a wide range of manipulation tasks.

We demonstrated successful adhesion of the biomimetic disc to household items (figures 1(e)–(j) and (k)–(o)), where surface geometries, textures, and weights varied. While suspended in air, the suction disc supported bottles of preserved goods (450 g, mass in air) and fresh produce, including oranges (250 g), bell peppers (240 g), tomatoes (210 g), strawberries (38 g), and cherries (9 g). While suspended in water, the suction disc gripped ceramic pitchers (320 g, mass in water), calcareous shells (210 g), a Dungenous crab (2 g), a textured ceramic vase (320 g), and a golf ball (6 g). Deformation of the biomimetic disc was the only method of initiating suction in both air and water trials. No additional actuation was required to sustain grip. The ability to deform to the variable surfaces and maintain a vacuum in the suction chamber yielded success at picking up and holding the objects of interest.

To further the application of manipulation, we sought to provide a soft touch to the manipulators of ROVs, which are designed for industrial applications but are also used for subsea recovery of specimen and archaeological artifacts. Manipulators used by ROVs, such as the Kraft Predator (80 kg, 1334 N maximum grip force) [52] (figure 15(a)), do not have a soft touch; this fact increases the risk of damaging delicate

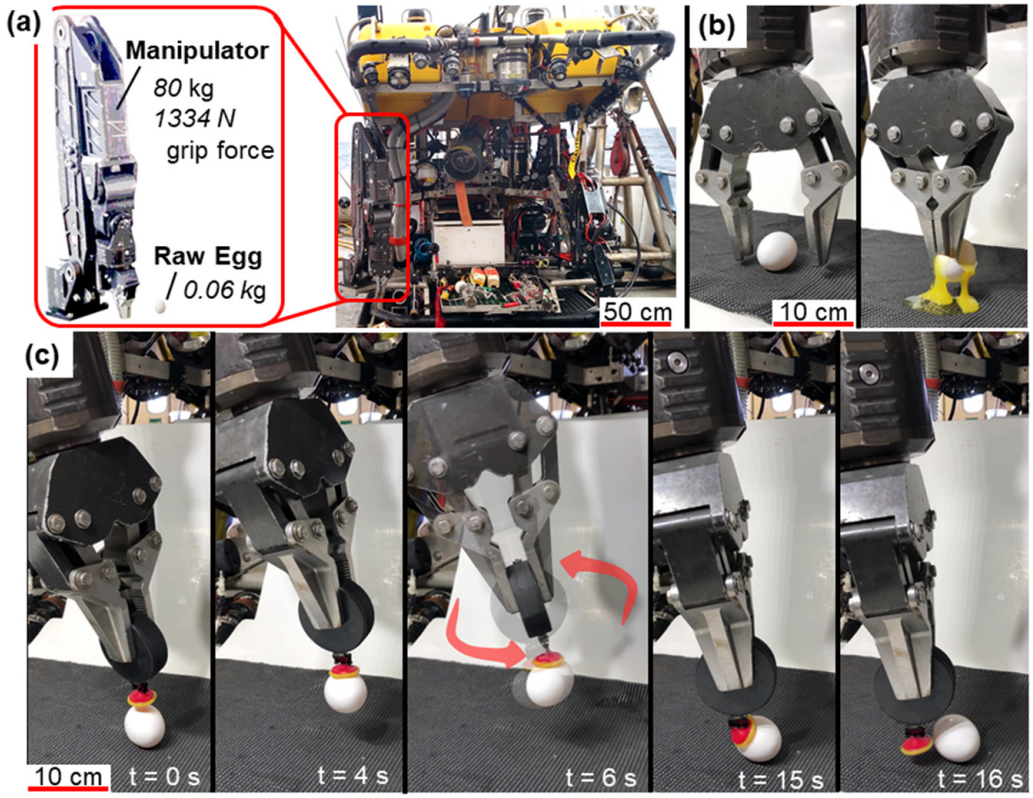

Figure 15. Providing soft touch to an ROV manipulator. (a) Overview of the subsea manipulator used by ROV Hercules. (b) Unsuccessful attempt to grip a raw egg without use of suction disc. (c) Manipulator using a suction disc to successfully grip, rotate (x3) and replace raw egg without damage.

artifacts. We addressed this challenge by designing a passive adaptor equipped with a suction disc for use by the manipulators of underwater vehicles. As a proof of concept, two experienced pilots attempted to manipulate a raw egg both with and without the suction disc using the robotic manipulator (movie S5). By fixing the disc to a hard handle, we were able to successfully adhere to, pick up, perform three full rotations, and place a raw egg (0.06 kg) back on a surface without damage (figure 15(c)). We disengaged the biomimetic disc by moving the manipulator tangential to the egg surface. By comparison, trials without the use of a suction disc were unsuccessful at manipulating the egg without significant damage to the fragile object (figure 15(b)). Although the trials were performed using a subsea manipulator in air, we were able to demonstrate the capability of the manipulator to successfully manipulate a delicate raw egg using our suction disc.

4. Discussion

By combining insights from engineering and biology, we developed an artificial mimic of the suction disc of the northern clingfish. Upon initial experimentation with the biological specimen, we observed that a euthanized clingfish can withstand normal loads yet was unable to resist shear forces against a wet glass surface. We therefore engineered a mimic of the clingfish with the ability to withstand normal loads on rough and irregular surfaces while being passive in mechanism.

The biological mechanisms of adhesion of the clingfish are highly complex. However, we hypothesize that similar adhesion can be achieved with a simplified design consisting of a suction chamber with a soft layer covering the disc margin to allow for sealing to irregular surfaces. Our observations support the previous conclusion that the soft fibrils that originate from an extensive network of papillae provide one of the primary mechanisms by which the low-pressure chamber is sealed [42].

We mimicked the microfeatures of the suction disc of the clingfish and also approximated their function. In order to mimic the fibrils of the clingfish originating from the papillae, we fabricated artificial discs lined with microscopic silicone pillars. Overall, the discs with micropillars that were composed of a soft silicone were better capable at adhering to surfaces in comparison to the prototypes with pillars of stiff silicone. The soft micropillars were capable of intermeshing together, the overlap thereby sealing in gaps of the disc margin that could otherwise compromise the chamber of subatmospheric pressure. A similar mechanism of sealing may occur in the clingfish where the fibrils of the papillae intermesh to generate a thicker, seemingly continuous soft layer of the disc margin.

Our preliminary work demonstrated that the suction discs with micropillars performed worse in

comparison to suction discs without micropillars, most notably on rough surfaces underwater. However, the suction disc with soft micropillars were more successful at adhering to all surfaces in air and underwater, in comparison to the disc with stiff micropillars. This finding coupled with micrographs of the artificial micropillars suggests that the soft micropillars acted to intermesh together, generating a seemingly thicker soft disc margin. The intermeshing behavior would thereby more effectively seal the suction chamber. We acknowledge that in this study, the micropillars were approximated but not optimized in geometry or spacing, and could therefore be improved to better mimic the microscale geometry of the fibrils of clingfish, which may lead to greater sealing performance.

Our bioinspired suction discs outperformed commercial suction cups on rough textures and concave surfaces. In air, the discs with a soft layer, without micropillars, and without slits performed best on dry, rough surfaces. The biomimetic discs also supported large payloads both in and out of the water. In water, the discs with a soft layer and slits (without micropillars) outperformed all other prototypes and a commercially available suction cup on moderate and coarse surfaces. The biomimetic discs sustained higher adhesive stresses in water than in air. We coupled these results with the comparison of wet and dry surface contact, as visualized by FTIR. The suction disc was able to retain a circular shape of its perimeter when subject to load on a wet surface. Conversely, when the disc was subjected to the same load on a dry surface, the perimeter elongated to an ellipse. Elongation was hypothesized to be the result of the disc margin anchoring to the dry surface. We concluded that the suction disc on the wetted surface would be lubricated by a thin fluid film, resulting in the retention of the circular shape of the perimeter and thus a more even distribution of stress within the body when subjected to a load. The observations made by comparing FTIR results corresponded with the force measurements performed on surfaces in air and underwater. Thus, the higher adhesive stresses achieved by the suction disc in water may be in part due to boundary lubrication by a thin fluid film and a more even distribution of stress within the body cavity.

The performance of our suction discs on coarse surfaces underwater (grain size, 269 μm; 14.3 $\pm$ 1.4 kPa) was comparable to the performance of a biomimetic suction disc inspired by the remora ($R_a = 200$ μm, 15.8 $\pm$ 0.1 kPa, [41]). However, contrary to the remora-inspired disc, our design was unactuated, simplistic in fabrication, and passive in its ability to maintain adhesion.

Three components were identified as critical to improving adhesion: body geometry, a soft layer in the disc margin, and the presence of slits. Body symmetry affected adhesive capabilities of the suction disc. The bilaterally symmetric body performed worse in all occasions in comparison to the radially symmetric body. We concluded that the radial body geometry was capable of better distributing stress across the circumference of the body, allowing for improved adhesion, in comparison to the bilaterally symmetric body.

A soft layer in the disc margin improved performance on concave and rough surfaces. While the stiff silicone backing functioned to maintain the integrity of the internal suction chamber, a soft compliant layer of silicone in the disc margin greatly enhanced sealing capabilities to rough surfaces, similar to the hypothesized role of the soft fibrils originating from the papillae of the clingfish. As visualized using FTIR, the soft layer increased the effective area of contact between the disc and a surface. The relatively large area in contact with the imaging surface increased the frictional footprint of the biomimetic disc, thereby enhancing its capabilities for sealing and sustaining a chamber of low pressure.

The results from the longevity study also demonstrated the ability of the biomimetic disc with a soft layer to maintain a seal for a long period of time while bearing a payload. The suction disc with a soft layer and slits was more successful at bearing a load over an extended amount of time in comparison to the disc without a soft layer and to the commercial suction cup. The soft layer aided in the sealing of the suction chamber. The friction of the soft disc margin helped to prevent the inward slip of the perimeter of the suction disc, which would otherwise lead to failure of attachment. These two factors allowed for a larger payload to be supported by the disc and for a longer period of time, in comparison to the discs without a soft layer. The ability of a 2 g suction disc to bear a payload that is 191 times its mass for well over 100 min suggest that the disc may prove useful in load-bearing applications, such as in manipulation or semi-permanent fixtures.

Geometric and material compliance impacted adhesive capabilities to irregular surfaces. Adhesive discs with slits were considered more geometrically compliant in comparison to their counterparts without slits. Geometric compliance yielded better conformation of the disc to concave shapes to prevent the loss of vacuum from the low-pressure chamber. However, slits were less successful in comparison to material stiffness at maintaining adhesion to convex surfaces. Overall, adhesion to convex surfaces was positively influenced by stiffness of the disc margin and negatively influenced by slits. This trend was opposite that observed for concave surfaces, in which adhesion was positively influenced by slits and negatively influenced by stiffness of the disc margin. Coupling shape with roughness, discs with a soft margin and slits were most successful at adhering to rough, concave surfaces. The results from the rough, concave experimental surface demonstrated the combined effect of slits and a soft layer, which are individually most successful at maintaining adhesion to concave and rough surfaces, respectively.

We investigated the minimal preload required to achieve attachment to two substrates with different

values of surface roughness. The minimal preload to attach a disc to the smooth surface was 0.5 N and 1.5 N to the moderately rough surface (grain size, 68 μm). A greater preload suggested a more substantial deformation of the suction disc, thereby expelling a greater amount of fluid from the chamber, resulting in the storage of strain energy within the structure. The combination of a greater amount of expelled fluid and higher stored strain energy, subject to limitations, allowed for a larger pressure differential between internal and external environments. We hypothesize that a greater preload required for rough surfaces may also act to more forcibly conform the soft layer of the suction disc to surface asperities, thereby sealing the suction chamber. Greater conformation to the rough surface would result in an increased resistance to slip in the disc margin which would help to seal the low-pressure chamber.

The results from studying the minimal preload required for attachment suggested possible applications of the suction disc. Given that the preloads to achieve attachment were relatively low in comparison to other work on robotic grippers intended for delicate gripping tasks [53, 54] this could lead to applications that include manipulation of fragile objects. However, we only explored the preloads required for substrates with two values of surface roughness on exclusively hard surfaces. Future work could therefore explore the effect of preloads on non-rigid surfaces or under a variable environmental conditions.

The results from FEA suggested that the inverted state of the suction discs was energetically favored in all simulated cases when we applied a load of vertical compression. This finding corresponded with the behavior that we observed in FTIR when the suction disc without a soft layer inverted from the surface. We also observed that the presence of a soft layer impacted the tendency of a disc to invert. As demonstrated in FTIR, the disc with a soft layer did not invert, whereas a disc without a soft layer did invert.

We also used FEA to evaluate the impact of slits on the total strain energy of the system. The results from FEA showed that the discs with slits had a lower total strain energy in comparison to the discs without slits. The work done by the initial compression is either stored in the body as elastic potential energy or performs work on the fluid within the suction chamber, evacuating the chamber, and forming a vacuum. Therefore, for a given amount of work to engage the suction disc, we concluded that designs with lower energy storage will experience greater work done on the fluid, suggesting a higher adhesive force. When a force of detachment is applied to the disc, the total energy of the system consists of not only the stored elastic energy in the deformed body, but also the potential energy from the load applied to the disc and the interfacial surface energy used to separate a unit area of the disc from a surface [55]. Our models were used to understand deformation of the suction discs and do not account for other factors such as surface energies, friction, or vacuum, which are also important to adhesion.

Coupling observations from FEA and the experiments of preload, a higher preload resulted in a higher total stored elastic energy of the system. Given that we were only comparing the effect of preload on adhesive capabilities of one disc design (radially symmetric, with soft layer, without slits), the work done to the body of the suction disc was stored reversibly within the disc. We expect there to exist a trade-off of the magnitude of preload to adhesion. That is, a larger preload would result in a greater stored elastic potential energy and thus a greater restoring force. The preload would therefore have a threshold value that, when surpassed in magnitude, would be counterproductive to adhesion, resulting in a high restoring force that would lead to detachment of the disc from a surface via an elastic restoration to its original shape.

While the biomimetic discs worked well on adhering to concave shapes, coarse surfaces underwater, and moderately rough surfaces in air, they had limited performance on coarse surfaces in air and convex shapes with small radii of curvature. The performance of the suction discs was half of that reported for the biological specimen in previous studies on rough surfaces [44]. Additionally, the artificial suction discs were less successful at adhering to convex surfaces with comparison to concave. However, the clingfish is found to live on intertidal rocks, which we would suggest have both locally convex and concave features. We hypothesize that the ability of the clingfish to actively adjust its suction disc may influence its ability to adhere to irregular surfaces. Our artificial suction discs did not have an active mechanism by which to adjust its seal, which may contribute to its decreased adhesive capabilities to convex surfaces in comparison to the biological specimen. We suggest that while we were mimicking key components of the suction disc, such as geometry, we have left other components of adhesion, such as secretions, to future work. The clingfish is hypothesized to use secretions [44], much like gastropods [56], to increase the viscosity of the fluid beneath the organism, thereby increasing the contribution of Stefan adhesion to surface attachment.

The clingfish and the commercial suction cup achieved higher adhesive pressures on flat, smooth surfaces in comparison to the biomimetic discs. The pelvic girdle of the clingfish and the commercial suction cup are both stiffer than the bioinspired discs, thereby preventing deformation of the suction chamber when subjected to external pulling forces. Therefore, the stiffness in the backing also plays a role in achieving higher adhesive pressures. 3D reconstructions of the clingfish could therefore be used to inform designs of the suction disc to achieve higher adhesive stresses in future work.

In evaluating the adhesive performance of the prototypes, we only performed pull tests that were

normal to the experimental surface, analogous to the pull tests performed on clingfish specimen. Our suction discs, much like the euthanized clingfish, are much less capable of resisting shear forces while on wet glass surfaces. We did not test the combination of shear and normal forces on neither the clingfish nor the artificial suction discs, which we leave for future work. Applications in which high normal adhesion and low resistance to shear forces could be favorable include pick-and-place manipulations or adhesive footpads for robotic locomotion.

Future work could explore the modification of the suction disc geometry, size, composition, and surface structure of the disc margin to tailor its use to specific surfaces and external disturbances, such as fluid flow, for use in applications not explored here. Tailoring micropillar materials in the disc margin may also aid in adhesion in an underwater environment, as demonstrated by microstructured hydrogels to yield amphibious adhesion [36].

In sum, we created a suction disc that functions in and out of water to grip rough and irregular surfaces without necessitating sustained actuation. Our system is effective at gripping textured surfaces while being relatively simple and inexpensive to fabricate. The bioinspired design has many potential applications, including robotic manipulation. We demonstrated its capabilities on handling delicate objects, such as fresh produce, of varying weights and textures. With the suction disc, we can also provide a delicate touch to the seemingly ungentle, such as subsea manipulators. As demonstrated in this study, the suction disc gave a manipulator commonly used in subsea operations the ability to delicately maneuver a raw egg. Given these demonstrated capabilities, future iterations of the clingfish-inspired suction disc could markedly improve manipulation while being cost-effective for fabrication.

Acknowledgments

We thank MA Meyers (UCSD) and SQ Cai (UCSD) for providing feedback to this work and for use of their lab facilities. We thank N Gravish (UCSD) for use of FTIR imaging station and A Zonderman (Deheyn lab volunteer) for help in biological sample collection. We thank A Parness (JPL) and P Glick (UCSD) for use of micropillar molds. We thank Z Song, Y Wang, and SQ Cai for the use of their testing equipment. We thank the Ocean Exploration Trust for use of ROV Hercules aboard the E/V Nautilus, and ROV pilot T Shepherd for manipulation. Images from FEA courtesy of ANSYS, Inc.

Funding

This work is supported by the Office of Naval Research grant number N000141712062. J Sandoval is supported by the Gates Millennium Scholars (GMS) program. This work was facilitated by the Biomimicry for Emerging Science and Technology (BEST) Initiative .

Author contributions

JAS, MTT, and DDD conceived the project. JAS characterized the morphology of the clingfish suction disc. HQ performed scanning electron microscopy on the biological specimen. JAS designed and fabricated the clingfish-inspired disc. JAS performed and analyzed tests of adhesion of the biomimetic discs. SJ performed Finite Element Analysis of the suction discs. SJ performed longevity and preload experiments. JAS conducted robotic manipulation experiments. JAS prepared the initial draft of the manuscript and all authors provided feedback during revisions.

Competing interests

Invention disclosure UCSD# SD2019-160 (to JAS, DDD, MTT) has been filed describing fabrication and performance testing of the clingfish-inspired adhesive disc.

Data and materials availability

Please contact JAS for data and other materials.

ORCID iDs

Jessica A Sandoval https://orcid.org/0000-0002-7598-8135
Dimitri D Deheyn https://orcid.org/0000-0002-6496-9297
Michael T Tolley https://orcid.org/0000-0001-7821-7777

References

[1] Sun W, Neuzil P, Suryadi Kustandi T, Oh S and Samper V D 2005 The nature of the gecko lizard adhesive force *Biophys. J.: Biophys. Lett.* **89** L14–7
[2] Izadi H and Penlidis A 2013 Polymeric bio-inspired dry adhesives: van der Waals or electrostatic interactions? *Macromolec. React. Eng.* **7** 1–21
[3] Ditsche P and Summers A P 2014 Aquatic versus terrestrial attachment: Water makes a difference *Beilstein J. Nanotechnol.* **5** 2424–39
[4] Favi P M, Yi S, Lenaghan S C, Xia L and Zhang M 2014 Inspiration from the natural world: from bio-adhesives to bioinspired adhesives *J. Adhes. Sci. Tech.* **28** 290–19
[5] Brodoceanu D, Bauer C T, Kroner E, Arzt E and Kraus T 2016 Hierarchical bioinspired adhesive surfaces—a review *Bioinsp. Biomim.* **11** 051001
[6] Chuang Y C, Chang H K, Liu G L and Chen P Y 2017 Climbing upstream: multi-scale structural characterization and underwater adhesion of the Pulin river loach (*Sinogastromyzon puliensis*) *J. Mech. Behav. Biomed. Mater.* **73** 76–85
[7] Autumn K, Dittmore A, Santos D, Spenko M and Cutkosky M 2006 Frictional adhesion: a new angle on gecko attachment *J. Exp. Biol.* **209** 3569–79
[8] Santos R, Gorb S, Jamar V and Flammang P 2005 Adhesion of echinoderm tube feet to rough surfaces *J. Exp. Biol.* **208** 2555–67

[9] North M A, Del Grosso C A and Wilker J J 2017 High strength underwater bonding with polymer mimics of mussel adhesive proteins *ACS Appl. Mater. Interfaces* **9** 7866–72
[10] Lin A, Brunner R, Chen P, Talke F and Meyers M 2009 Underwater adhesion of abalone: the role of van der Waals and capillary forces *Acta Mater.* **57** 4178–5
[11] Heepe L and Gorb S N 2014 Biologically inspired mushroom-shaped adhesive microstructures *Ann. Rev. Mater. Res.* **44** 173–203
[12] Kesel A B, Martin A and Seidl T 2004 Getting a grip on spider attachment: an AFM approach to microstructure adhesion in arthropods *Smart Mater. Struct.* **13** 512–8
[13] Langowski J K A, Dodou D, Kamperman M and van Leeuwen J L 2018 Tree frog attachment: mechanisms, challenges, and perspectives *Frontiers Zool.* **15** 32
[14] Smith A M 1996 Cephalopod sucker design and the physical limits to negative pressure *J. Exp. Biol.* **199** 949–58
[15] Smith A M 1991 The role of suction in the adhesion of limpets *J. Exp. Biol.* **161** 151–69
[16] Barnes W J P 2007 Functional morphology and design constraints of smooth adhesive pads *MRS Bull.* **32** 479–85
[17] Autumn K, Liang Y A, Hsieh T S, Zesch W, Chan W P, Kenny T W, Fearing R and Full R J 2000 Adhesive force of a single gecko foot-hair *Nature* **405** 681–5
[18] Persson B N J 2007 Wet adhesion with application to tree frog adhesive toe pads and tires *J. Phys.: Condens. Matter* **19** 3761104
[19] Federle W, Riehle M, Curtis A S G and Full R J 2002 An integrative study of insect adhesion: Mechanics and wet adhesion of pretarsal pads in ants *Integr. Comp. Biol.* **42** 1100–6
[20] Gorb S N 1998 The design of the fly adhesive pad: distal tenent setae are adapted to the delivery of an adhesive secretion *Proc. R. Soc.* B **265** 747–52
[21] Federle W, Barnes W J P, Baumgartner W, Drechsler P and Smith J M 2006 Wet but not slippery: boundary friction in tree frog adhesive toe pads *J. R. Soc. Interface* **3** 689–97
[22] Culler M, Ledford K A and Nadler J H 2014 The role of topology and tissue mechanics in remora attachment *Mater. Res. Soc. Symp. Proc.* **1648** Mrsf13-1648-hh10-02
[23] Kampowski T, Eberhard L, Gallenmuller F, Speck T and Poppinga S 2016 Functional morphology of suction discs and attachment performance of the Mediterranean medicinal leech (*Hirudo verbana* Carena) *J. R. Soc. Interface* **13** 20160096
[24] Gorb S N 2009 Biological attachment devices: exploring nature's diversity for biomimetics *Phil. Trans. R. Soc.* A **366** 1557–74
[25] Li Y, Krahn J and Menon C 2016 Bioinspired dry adhesive materials and their application in robotics: A review *J. Bionic Eng.* **13** 181–99
[26] Cutkosky M R 2015 Climbing with adhesion: from bioinspiration to biounderstanding *Interface Focus* **5** 20150015
[27] Calisti M, Picardi G and Laschi C 2017 Fundamentals of soft robot locomotion *J. R. Soc. Interface* **14** 20170101
[28] Zhou X, Majidi C and O'Reilly O M 2015 Soft hands: an analysis of some gripping mechanisms in soft robot design *Int. J. Solids Struct.* **65** 155–65
[29] Shintake J, Cacucciolo V, Floreano D and Shea H 2018 Soft robotic grippers *Adv. Mater.* **30** 1707035
[30] Daltorio K A, Wei T E, Horchler A D, Southard L, Wile G D, Gorb S N, Ritzmann R E and Quinn R D 2009 Mini-Whegs™ climbs steep surfaces using insect-inspired attachment mechanisms *Int. J. Robot. Res.* **28** 285–302
[31] Polygerinos P, Correll N, Morin S A, Mosadegh B, Onal C D, Petersen K, Cianchetti M, Tolley M T and Shepherd R F 2017 Soft robotics: review of fluid-driven intrinsically soft devices; Manufacturing, sensing, control, and applications in human-robot interaction *Adv. Eng. Mater.* **19** 1700016
[32] Glick P, Suresh S A, Ruffatto D I, Cutkosky M, Tolley M T and Parness A 2018 A soft robotic gripper with gecko-inspired adhesive *IEEE Robot. Autom. Lett.* **3** 903–10
[33] Jiang H *et al* 2017 A robotic device using gecko-inspired adhesives can grasp and manipulate large objects in microgravity *Sci. Robot.* **2** eaan4545
[34] Song S, Drotlef D M, Majidi C and Sitti M 2017 Controllable load sharing for soft adhesive interfaces on three-dimensional surfaces *PNAS* **114** E4344–53
[35] Glass P, Chung H, Washburn N R and Sitti M 2009 Enhanced reversible adhesion of dopamine methacrylamide-coated elastomer microfibrillar structures under wet conditions *Langmuir* **25** 6607–12
[36] Yi H, Lee S H, Seong M, Kwak M K and Jeong H E 2018 Bioinspired reversible hydrogel adhesives for wet and underwater surfaces *J. Mater. Chem.* B **6** 8064–70
[37] Izadi H, Zhao B, Han Y, McManus N and Penlidis A 2012 Teflon hierarchical nanopillars with dry and wet adhesive properties *J. Polym. Sci.* B **50** 846–51
[38] Varenberg M and Gorb S 2008 A beetle-inspired solution for underwater adhesion *J. R. Soc. Interface* **5** 383–5
[39] Mazzolai B, Margheri L, Cianchetti M, Dario P and Laschi C 2012 Soft-robotic arm inspired by the octopus: II. From artificial requirements to innovative technological solutions *Bioinspir. Biomim.* **7** 025005
[40] Tramacere F, Follador M, Pugno N M and Mazzolai B 2015 Octopus-like suction cups: from natural to artificial solutions *Bioinsp. Biomim.* **10** 035004
[41] Wang Y *et al* 2017 A biorobotic adhesive disc for underwater hitchhiking inspired by the remora suckerfish *Sci. Robot.* **2** eaan8072
[42] Green D M and Barber L D 1987 The ventral adhesive disc of the clingfish *Gobiesox maeandricus*: integumental structure and adhesive mechanisms *Canad. J. Zool.* **66** 1610–9
[43] Ditsche P, Wainwright D K and Summers A P 2014 Attachment to challenging substrates—fouling, roughness and limits of adhesion in the northern clingfish (*Gobiesox maeandricus*) *J. Exp. Biol.* **217** 2548–54
[44] Wainwright D K, Kleinteich T, Kleinteich A, Gorb S N and Summers A P 2013 Stick tight: suction adhesion on irregular surfaces in the northern clingfish *Biol. Lett.* **9** 20130234
[45] Schneider C A, Rasband W S and Eliceiri K W 2012 NIH Image to ImageJ: 25 years of image analysis *Nat. Met.* **9** 671–5
[46] Yap H K, Goh J C H and Yeow R C H 2015 Design and characterization of soft actuator for hand rehabilitation appplication *6th European Conf. of the Int. Federation for Medical and Biological Engineering Proc.* **45** 367–70
[47] Park Y L, Majidi C, Kramer R, Bérard P and Wood R J 2010 Hyperelastic pressure sensing with liquid-embedded elastomer *J. Micromech. Microeng.* **20** 125029
[48] Parness A, Soto D, Esparza N, Gravish N, Wilkinson M, Autumn K and Cutkosky M 2009 A microfabricated wedge-shaped adhesive array displaying gecko-like dynamic adhesion, directionality and long lifetime *J. R. Soc. Interface* **6** 1223–32
[49] Noor M M, Kadirgama K and Rahman M M 2010 Analysis of surface roughness for laser cutting on acrylic sheets using response surface method *Nat. Conf. Mech. Eng. Res. Postgrad. Stud.* **1** 24–31
[50] Han J Y 2005 Low-cost multi-touch sensing through frustrated total internal reflection *UIST Proceed.* **18** 115–8
[51] Hertzberg R W, Vinci R P and Hertzberg J L 2013 Elastic response of solids *Deformation and Fracture Mechanics of Engineering Materials* (New Jersey: Wiley) pp 3–61
[52] Kraft TeleRobotics, Inc. 2005 Predator: force feedback manipulator *Product Specification P505-1* Kraft TeleRobotics
[53] Maruyama R, Watanabe T and Uchida M 2013 Delicate grasping by robotic gripper with incompressible fluid-based deformable fingertips *IEEE Int. Conf. Intel. Rob. Sys.* 5469–74
[54] Krahn J M, Fabbro F and Menon C 2017 A soft-touch gripper for grasping delicate objects *IEEE/ASME Trans. Mechatron.* **22** 1276–86
[55] Kendall K 1971 The adhesion and surface energy of elastic solids *J. Phys. D: Appl. Phys.* **4** 1186–95
[56] Lai J H, del Alamo J C, Rodríguez-Rodríguez J and Lasheras J C 2010 The mechanics of the adhesive locomotion of terrestrial gastropods *J. Exp. Biol.* **213** 3920–33